

Universality of jamming of non-spherical particles

Carolina Brito^a, Harukuni Ikeda^{b,1}, Pierfrancesco Urbani^c, Matthieu Wyart^d, and Francesco Zamponi^b

^aInstituto de Física, UFRGS, 91501-970, Porto Alegre, Brazil; ^bLaboratoire de physique théorique, Département de physique de l'ENS, École normale supérieure, PSL University, Sorbonne Université, CNRS, 75005 Paris, France; ^cInstitut de physique théorique, Université Paris Saclay, CNRS, CEA, F-91191 Gif-sur-Yvette, France; ^dInstitute of Physics, EPFL, CH-1015 Lausanne, Switzerland

This manuscript was compiled on November 30, 2021

Amorphous packings of non-spherical particles such as ellipsoids and spherocylinders are known to be hypostatic: the number of mechanical contacts between particles is smaller than the number of degrees of freedom, thus violating Maxwell's mechanical stability criterion. In this work, we propose a general theory of hypostatic amorphous packings and the associated jamming transition. First, we show that many systems fall into a same universality class. As an example, we explicitly map ellipsoids into a system of "breathing" particles. We show by using a marginal stability argument that in both cases jammed packings are hypostatic, and that the critical exponents related to the contact number and the vibrational density of states are the same. Furthermore, we introduce a generalized perceptron model which can be solved analytically by the replica method. The analytical solution predicts critical exponents in the same hypostatic jamming universality class. Our analysis further reveals that the force and gap distributions of hypostatic jamming do not show power-law behavior, in marked contrast to the isostatic jamming of spherical particles. Finally, we confirm our theoretical predictions by numerical simulations.

jamming | glass | marginal stability | non-spherical particles

Upon compression, an athermal system consisting of purely repulsive particles suddenly acquires finite rigidity at a certain jamming transition density φ_J at which constituent particles start to touch each other producing a finite mechanical pressure (1–3). The jamming transition is observed in a wide variety of physical, engineering and biological systems such as metallic balls (4), foams (5, 6), colloids (7), polymers (8), candies (9), dices (10) and tissues (11). In the past decade, a lot of progress has been made in understanding the jamming transition of spherical and frictionless particles with repulsive interactions. Key findings involve (i) the power law behaviors of the elastic modulus and contact number as a function of the proximity to φ_J (6, 12, 13), (ii) the emergence of excess soft modes in the vibrational density of states $D(\omega)$ (6), and (iii) the power law divergence of the gap distribution function $g(h)$ and power law tail of the force distribution function $P(f)$ at φ_J (6, 14–16). Those phenomena can be understood in terms of a marginal stability principle (17, 18): the system lies close to a mechanical instability. More precisely, at φ_J , the contact number per particle is $z_J = 2d$ (4, 6), which barely satisfies the Maxwell's mechanical stability condition (19). Accepting marginal stability as a basic principle, one can successfully predict the critical exponents of soft spheres (17, 18) and derive a scaling relation between critical exponents of hard spheres (20–23). The importance of marginal stability is also highlighted by exact calculations for hard spheres in the large dimension limit (15) and in a perceptron model of the jamming transition (24–26). These first principle calculations prove that a full replica symmetric breaking (RSB) phase transition occurs ahead of the

jamming transition. In the full RSB phase, the eigenvalue distribution function is gapless, and thus, the system is indeed marginally stable (24). This approach provides exact results for the critical exponents, which agree well with the numerical results (15), once localized excitation modes are carefully separated (16, 22).

However, a system of spherical particles is an idealized model and, in reality, constituent particles are, in general, non-spherical. In this case, one should specify the direction of each particle in addition to the particle position. The effects of those extra degrees of freedom have been investigated in detail in the case of ellipsoids (2, 3, 9, 27–32). Notably, the contact number at the jamming point continuously increases from the isostatic value of spheres, as $z_J - 2d \propto \Delta^{1/2}$, where Δ denotes the deviation from the perfectly spherical shape. The system is thus *hypostatic*: the contact number is lower than what expected by the naive Maxwell's stability condition, which would predict $z_J = 2(d + d_{\text{ex}})$ where d_{ex} is the number of rotational degrees of freedom per particle (9, 28, 29). As a consequence of hypostaticity, $D(\omega)$ has anomalous zero modes at φ_J , which are referred to as "quartic modes" because they are stabilized by quartic terms of the potential energy (29–32). Hypostatic packings are also obtained for spherocylinders (33–37), superballs (38), superellipsoids (39), other convex shaped particles (40) and even deformable polygons (41). Compared to spherical particles, the theoretical understanding of the jamming transition of non-spherical particles is still in its infancy (29, 42). In particular, the physical mechanism that induces a scaling behavior such as $z_J - 2d \propto \Delta^{1/2}$ is unclear.

In this work, we propose a theoretical framework to describe the universality class of hypostatic jamming. As a first example of universality, we will map ellipsoids into a model

Significance Statement

The jamming transition is a key property of granular materials, including sand and dense suspensions. In the generic situation of non-spherical particles, its scaling properties are not completely understood. Previous empirical and theoretical work in ellipsoids and spherocylinders indicates that both structural and vibrational properties are fundamentally affected by shape. Here we explain these observations using a combination of marginal stability arguments and the replica method. We unravel a new universality class for particles with internal degrees of freedom, and derive how the structure of packings and their vibrations scale as the particles evolve toward spheres.

B.C., H.I., P.U., M.W. and F.Z. designed research, performed research, and wrote the paper.

The authors declare no conflict of interest.

¹To whom correspondence should be addressed. E-mail: harukuni.ikeda@lpt.ens.fr

of “breathing” spherical particles (BP), recently introduced in (43). Based on the mapping, we show that the two models indeed have the same critical exponents by using a marginal stability argument. Next, we propose a generalisation of the random perceptron model that mimics the BP and can be solved analytically using the replica method. We confirm that this model is in the same universality class of ellipsoids, BP, and other non-spherical particles that display hypostatic jamming. This analysis further predicts the scaling behavior of $g(h)$ and $P(f)$ near the jamming point. Interestingly, we find that these functions do not show a power-law behavior even at the jamming point, in marked contrast to the jamming of spherical particles. Also the simplicity of the model allows us to derive an analytical expression of the density of states $D(\omega)$, which exhibits the very same scaling behavior of that of ellipsoids and BP. Finally, we confirm our predictions by numerical simulations of the BP model.

Breathing particles model – The BP model (43) was originally introduced to understand the physics of the Swap Monte Carlo algorithm (44), but here we will focus on its relation with the jamming of ellipsoids. The model consists of N spherical particles with positions \mathbf{x}_i in d -dimensions and radius $R_i \geq 0$, interacting via the potential energy:

$$V_N(\{\mathbf{x}\}, \{R\}) = U_N(\{\mathbf{x}\}, \{R\}) + \mu_N(\{R\}), \quad [1]$$

where, defining $\theta(x)$ as the Heaviside theta function,

$$U_N = \sum_{i < j} k \frac{h_{ij}^2}{2} \theta(-h_{ij}), \quad h_{ij} = |\mathbf{x}_i - \mathbf{x}_j| - R_i - R_j, \quad [2]$$

is the standard harmonic repulsive interaction potential of spherical particles such as bubbles and colloids (5), and the distribution of R_i , which can fluctuate around a reference value R_i^0 , is controlled by the chemical potential term:

$$\mu_N = \frac{k_R}{2} \sum_i (R_i - R_i^0)^2 \left(\frac{R_i^0}{R_i} \right)^2. \quad [3]$$

Here, k_R is determined by imposing that the dimensionless standard deviation $\Delta \propto \sqrt{\sum_i (R_i - R_i^0)^2 / (NR_0^2)}$ is constant, with $R_0 = N^{-1} \sum_i R_i^0$. Note that $\Delta = 0$ (corresponding to $k_R = \infty$) gives back the usual spherical particles (5), and that the full distribution of radii, $P(R)$, can generically change even if Δ is kept fixed. Upon approaching jamming, where the adimensional pressure p (in units of kR_0^{2-d}) vanishes, it is found that $k_R = p/\Delta$ and $P(R)$ remains constant (43).

Because the BP model has Nd translational degrees of freedom and N radial degrees of freedom, the naive Maxwell stability condition requires $z \geq 2(d+1)$ in the thermodynamic limit (19, 45). However, a marginal stability argument and numerical simulations prove that the contact number at the jamming point z_J increases continuously as $z_J - 2d \propto \Delta^{1/2}$ (43) and the system is hypostatic for sufficiently small Δ , *i.e.*, the number of constraints is smaller than that required by the Maxwell’s stability condition. This is very similar to ellipsoids and motivates us to conjecture that the two models could belong to the same universality class. In the following, we show that this expectation is indeed true: hypostatic packings of the BP and ellipsoids are stabilized by a common mechanism and have the same critical exponents.

Mapping from ellipsoids to BP – We now construct a mapping from a system of ellipsoids to the spherical BP model introduced above. Ellipsoids are described by their position \mathbf{x}_i and by unit vectors $\hat{\mathbf{u}}_i$ along their principal axis, and for concreteness, we model them by the Gay-Berne potential (31, 46):

$$V_N(\{\mathbf{x}\}, \{\hat{\mathbf{u}}\}) = \sum_{i < j} v(h_{ij}), \quad v(h) = k \frac{h^2}{2} \theta(-h), \quad [4]$$

where the gap function is defined as

$$h_{ij} = \frac{|\mathbf{x}_i - \mathbf{x}_j| - \sigma_{ij}}{\sigma_0}, \quad \frac{\sigma_{ij}}{\sigma_0} = \frac{1}{\sqrt{1 - \frac{\chi}{2} \left(\frac{(\hat{\mathbf{r}}_{ij} \cdot \hat{\mathbf{u}}_i + \hat{\mathbf{r}}_{ij} \cdot \hat{\mathbf{u}}_j)^2}{1 + \chi \hat{\mathbf{u}}_i \cdot \hat{\mathbf{u}}_j} + \frac{(\hat{\mathbf{r}}_{ij} \cdot \hat{\mathbf{u}}_i - \hat{\mathbf{r}}_{ij} \cdot \hat{\mathbf{u}}_j)^2}{1 - \chi \hat{\mathbf{u}}_i \cdot \hat{\mathbf{u}}_j} \right)}}. \quad [5]$$

Here, $\hat{\mathbf{r}}_{ij} = (\mathbf{x}_i - \mathbf{x}_j) / |\mathbf{x}_i - \mathbf{x}_j|$ is the unit vector connecting the i -th and j -th particles, $\varepsilon \sigma_0$ is the length of the principal axis, and $\chi = (\varepsilon^2 - 1) / (\varepsilon^2 + 1)$, where ε denotes the aspect ratio. Because we are interested in the nearly spherical case, we expand the pair potential in small $\Delta = \varepsilon - 1$ as

$$v(h_{ij}) = v(h_{ij}^{(0)}) - \frac{\Delta}{2} v'(h_{ij}^{(0)}) [(\hat{\mathbf{r}}_{ij} \cdot \hat{\mathbf{u}}_i)^2 + (\hat{\mathbf{r}}_{ij} \cdot \hat{\mathbf{u}}_j)^2] + \Delta^2 w_{ij}, \quad [6]$$

where $h_{ij}^{(0)} = r_{ij} / \sigma_0 - 1$ and $\Delta^2 w_{ij}$ denotes the $O(\Delta^2)$ term that we do not need to write explicitly. Substituting this in Eq. (4) and keeping terms up to Δ^2 , we obtain $V_N \approx U_N + \mu_N$, where

$$U_N = \sum_{i < j} \left[v(h_{ij}^{(0)}) + \Delta^2 w_{ij} \right], \quad \mu_N = \frac{1}{2} \sum_i (\Delta \hat{\mathbf{u}}_i) \cdot k_i \cdot (\Delta \hat{\mathbf{u}}_i). \quad [7]$$

The stiffness matrix is $k_i^{ab} = -\Delta^{-1} \sum_{j(\neq i)} v'(h_{ij}^{(0)}) \hat{\mathbf{r}}_{ij}^a \hat{\mathbf{r}}_{ij}^b$, where $a, b = 1, \dots, d$. Note that near the jamming point, k_i behaves as $k_i \sim v'(h) / \Delta \sim p / \Delta$, which is the same scaling of the stiffness k_R of the BP model, Eq. (3). Hence, if we identify $\Delta \hat{\mathbf{u}}_i$ with R_i , in the vicinity of jamming the potential for ellipsoids can be analyzed essentially in the same way as the BP model (43), as we discuss next.

Marginal stability – The distinctive feature of both BP and ellipsoids is that the total potential, and thus the Hessian matrix, can be split in two parts: one having finite stiffness, and the second having vanishing stiffness p/Δ by dimensional arguments. The zero modes of the first term are stabilized by the second, as recognized in Refs. (29, 32). We now provide additional insight on this structure by generalizing a marginal stability argument discussed for the BP in Ref. (43). At jamming, $p = 0$ and $V_N = U_N$ because $\mu_N \propto p$. The $\mathcal{N}_3 \equiv Nz/2$ constraints coming from U_N , one per mechanical contact, stabilize the same number of vibrational modes. Because the system is hypostatic, there remain $\mathcal{N}_0 \equiv N(d + d_{\text{ex}}) - Nz/2 = N(d_{\text{ex}} - \delta z/2)$ zero-frequency modes, where $\delta z = z - 2d$ and d_{ex} is the number of extra degree of freedom per particle, *i.e.*, $d_{\text{ex}} = 1$ for the BP and $d_{\text{ex}} = d - 1$ for ellipsoids. Above jamming, where $p > 0$, the \mathcal{N}_0 zero modes are stabilized by the “soft” constraint coming from μ_N whose characteristic

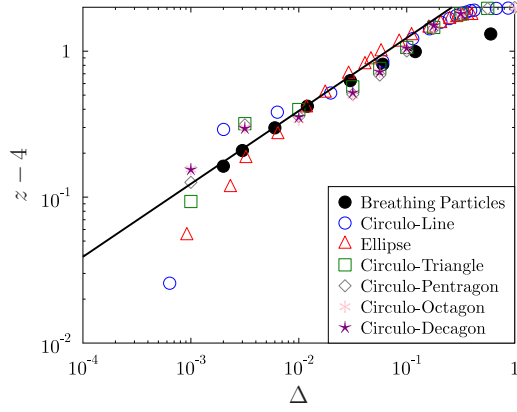


Fig. 1. Universal scaling of the contact number – Markers denote the numerical result, while the full line denotes the theoretical prediction $\delta z \sim \Delta^{1/2}$. Data for non-spherical particles are reproduced from Ref. (40), and from the sphericity A , we defined $\Delta = c(A - 1)^{1/2}$, which recovers the correct scaling relation between the sphericity and aspect ratio of ellipsoids for small Δ . We set $c = 1/6$ to collapse all data. Data for the BP correspond to a pressure $p = 10^{-6}$.

stiffness is $k_R \sim k_i \sim k(p/\Delta) \ll k$, where k is the stiffness associated to U_N . Hence, the energy scale of these modes remains well separated from that of the \mathcal{N}_3 other modes, and we can restrict to the \mathcal{N}_0 -dimensional subspace of the soft modes. In this space, we have $\mathcal{N}_0 = N(d_{\text{ex}} - \delta z/2)$ degrees of freedom, and μ_N provides Nd_{ex} constraints, hence the number of degrees of freedom is $N\delta z/2$ less than the number of constraints. When $\delta z \ll 1$, a variational argument was developed in (17, 47) to describe the low-frequency spectrum. It shows that the soft modes are shifted above a characteristic frequency $\omega_*^2 \sim k_i \delta z^2 \sim k_R \delta z^2 \sim \Delta^{-1} p \delta z^2$, which is reduced by $\sim -p$ by the so-called pre-stress terms, resulting in $\omega_*(p)^2 = c_1 \Delta^{-1} p \delta z^2 - c_2 p$, where c_1 and c_2 are unknown constants. Assuming that the system is marginally stable, $\omega_*(p) = 0$, results in (43)

$$\delta z \sim \Delta^{1/2}. \quad [8]$$

This explains the universal square root singularity of the contact number z_J observed in ellipsoids, BP and several other models (9, 29, 43), as illustrated in Fig. 1. Eq. (8) holds when $p \ll \Delta$, because in the argument we assumed to be close to jamming ($p \sim 0$) at fixed Δ . On the contrary, when $\Delta \ll p$, the contact number should have the same scaling of spherical particles:

$$\delta z \sim p^{1/2}. \quad [9]$$

Eqs. (8) and (9) imply that p and Δ have the same scaling dimension and the following scaling holds:

$$\delta z = \Delta^\gamma f(p/\Delta). \quad [10]$$

In the $\Delta \rightarrow 0$ limit, Eq. (10) reduces to Eq. (9), which requires $\gamma = 1/2$ and $f(x) \rightarrow x^{1/2}$ for $x \gg 1$. In the $p \rightarrow 0$ limit, we should recover Eq. (8), which requires $f(x) \rightarrow \text{const}$ for $x \ll 1$. For the BP, Eq. (10) is confirmed by numerical simulations (43). Assuming that $f(x)$ is a regular function around $x \sim 0$, one can expand it as $f(x) = c_0 + c_1 x + \dots$ and obtains

$$z - z_J \sim \Delta^{-1/2} p, \quad [11]$$

where $z_J = 2d + c_0 \Delta^{1/2}$. This is compatible with previous numerical results of ellipsoids, where $z - z_J \sim \Delta^{-0.35 \pm 0.1} p$ (48). We can also study the response to shear deformation, which mainly excites the zero-modes (30). Applying the argument in Ref. (18) to the zero-modes and using Eq. (8), the shear modulus G behaves as $G \sim \delta z k_R \sim \delta z k_i \sim p/\sqrt{\Delta}$, in perfectly agreement with the numerical result (30).

Vibrational spectrum – The marginal stability argument suggests that \mathcal{N}_0 soft vibrational modes can be found in the frequency range $\omega^* \lesssim \omega \lesssim \sqrt{k_R}$, with $\omega^* \sim 0$ due to marginal stability and $k_R \sim p/\Delta$, while the remaining \mathcal{N}_3 modes have finite frequency at jamming. We now refine the argument to discuss in more details the vibrational density of states $D(\omega)$. It is convenient to define the $\mathcal{N} \times \mathcal{N}$ Hessian matrix of the BP model, with $\mathcal{N} = N(d + d_{\text{ex}})$, as the second derivative of the interaction potential V_N w.r.t. \mathbf{x}_i and R_i/Δ , in such a way that it has a similar scaling of the one of ellipsoids, where R_i/Δ is mapped onto the angular degrees of freedom $\hat{\mathbf{u}}$.

Then, $D(\omega)$ near jamming can be separated into the following three regions. (i) The lowest band corresponds to the $\mathcal{N}_0 = N(d_{\text{ex}} - \delta z/2)$ zero modes stabilized by μ_N . Their typical frequency is $\omega_0^2 \sim \partial^2 \mu_N / \partial (\Delta^{-1} R_i)^2 \sim k_R \Delta^2 \sim \Delta p$. The remaining $\mathcal{N}_3 = \mathcal{N} - \mathcal{N}_0 = N\delta z/2$ modes can be split into two bands: (ii) an intermediate band corresponding to the extra (rotational or radial) degrees of freedom $\mathcal{N}_1 = N\delta z/2$, with typical frequency $\omega_1^2 \sim \partial^2 V_N / \partial (\Delta^{-1} R_i)^2 \sim \Delta^2$, and (iii) the highest band corresponding to the $\mathcal{N}_2 = Nd$ translational degree of freedom. For $\Delta \ll 1$, the additional degrees of freedom do not strongly affect these modes, and one can apply the standard variational argument of spherical particles (17, 47), which predicts that their typical frequency is $\omega_2^2 \sim \delta z^2 \sim \Delta$. The resulting $D(\omega)$ differs significantly from that of isotatic packings of spherical particles, which displays a single translational band.

Numerical results for $D(\omega)$ of ellipsoids from (30), of the BP from (43), and analytical results for the perceptron model to be introduced below, are reported in Fig. 2. Details about the simulations of the BP are explained in (43); here we show data for $N = 484$ particles, averaged over at least 1000 samples for each state point. As predicted by our theory, $D(\omega)$ consists of three separated bands with characteristic peak frequencies $\omega_{0,1,2}$. Their scaling with Δ , also reported in Fig. 2 at fixed p , follows the theoretical predictions $\omega_0 \propto \Delta^{1/2}$, $\omega_1 \propto \Delta$ and $\omega_2 \propto \Delta^{1/2}$. We also find that $\omega_0 \propto p^{1/2}$ for small p , while $\omega_{1,2}$ do not change much with p , which is again consistent with the theory. Finally, in Fig. 3 we report the fraction $f_i = \mathcal{N}_i/\mathcal{N}$ of modes in each band for the BP, which also follow the theoretical prediction as a function of Δ and p .

Mean field model – The universality class of isotatic jamming is well understood: it can be described analytically by particles in $d \rightarrow \infty$ (15) or, equivalently, by the perceptron model (24–26): both models reproduce the critical exponents of isotatic jamming in all dimensions d , leading to the conjecture that its lower critical dimension is $d = 2$ (49).

We now introduce a new mean field model which describes the universality class of hypostatic jamming in the BP, ellipsoids and many other models of non-spherical particles. The model, which is a generalization of the perceptron, can be solved analytically and, as we shall show, the solution reproduces all the critical exponents of hypostatic jamming. It

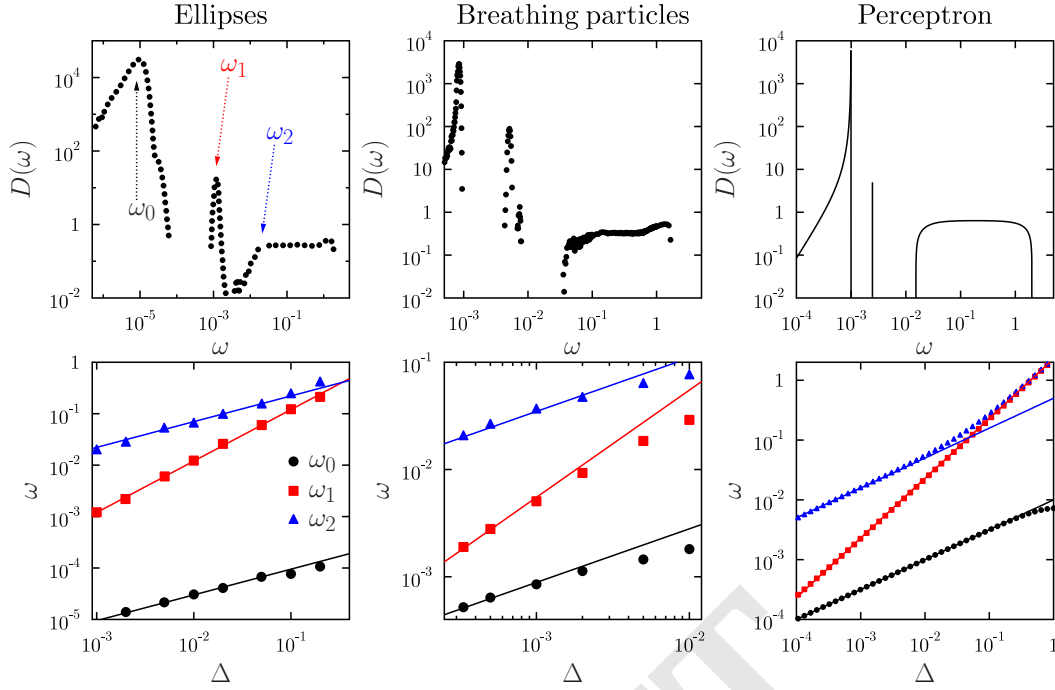


Fig. 2. Universality of the density of states – (Top) Density of states for ellipses, breathing particles, and the perceptron. (Bottom) Evolution with Δ of the characteristic frequencies at $p = 10^{-4}$. Full lines denote the theoretical predictions, $\omega_0 \propto \Delta^{1/2}$, $\omega_1 \propto \Delta$ and $\omega_2 \propto \Delta^{1/2}$, respectively. Data of ellipses are reproduced from Ref. (32).

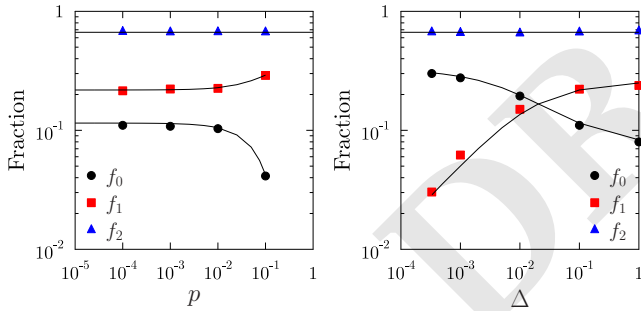


Fig. 3. Weights of the density of states – Fraction of modes $f_i = N_i/N$ in the three bands of $D(\omega)$ given in Fig. 2, plotted as functions of p at fixed $\Delta = 10^{-1}$ (left) and Δ at fixed $p = 10^{-4}$ (right) for breathing particles (with $d = 2$ and $d_{\text{ex}} = 1$). The theoretical predictions $f_0 = (1 - \delta z/2)/3$, $f_1 = \delta z/6$ and $f_2 = 2/3$ are plotted as full lines, inferred from the measured δz .

consists of one tracer particle with coordinate \mathbf{x} on the surface of the N dimensional hypersphere of radius \sqrt{N} , and M obstacles of coordinates ξ_μ and “size” $\sigma + R_\mu$. The interaction potential between the tracer particle and the obstacles is

$$V_N = U_N + \mu_N, \quad U_N = \sum_{\mu=1}^M v(h_\mu), \quad \mu_N = \frac{k_R}{2} \sum_{\mu=1}^M R_\mu^2, \quad [12]$$

where $v(h) = h^2\theta(-h)/2$ and the gap variable h_μ is defined as

$$h_\mu = \frac{\mathbf{x} \cdot \xi_\mu}{\sqrt{N}} - \sigma - R_\mu. \quad [13]$$

The ξ_μ are frozen variables, and each of their components follows independently a normal distribution of zero mean and

unit variance. The dynamical variables are \mathbf{x} and the R_μ , whose variance is controlled by the chemical potential μ_N . We fix the value of k_R so that $\sum_{\mu=1}^M R_\mu^2 = M\Delta^2$. In the $\Delta \rightarrow 0$ limit, the system reduces to the standard perceptron model investigated in Ref. (26), while for $\Delta > 0$ the R_μ play the same role of the particle sizes in the BP model.

Because the model can be solved by the same procedure of the standard perceptron model, here we just give a brief sketch of our calculation, which will be given in a longer publication. The free energy of the model at temperature $T = 1/\beta$ can be calculated by the replica method, $-\beta f = \lim_{n \rightarrow 0} \frac{1}{nN} \log \overline{Z^n}$, where $Z = \int d^N \mathbf{x} d^M \text{Re}^{-\beta V_N}$ and the overline denotes the averaging over the quenched randomness ξ_μ . Here we are interested in the athermal limit $T \rightarrow 0$. Using the saddle point method, the free energy can be expressed as a function of the overlap $q_{ab} = \langle \mathbf{x}^a \cdot \mathbf{x}^b \rangle / N$, where \mathbf{x}^a and \mathbf{x}^b denote the positions of the tracer particles of the a -th and b -th replicas, respectively. In the $n \rightarrow 0$ limit, q_{ab} is parametrized by a continuous variable $x \in [0, 1]$, $q_{ab} \rightarrow q(x)$. The function $q(x)$ plays the role of the order parameter and characterizes the hierarchical structure of the metastable states (50). We first calculate the phase diagram assuming a constant $q(x) = q$, which is the so-called replica symmetric (RS) ansatz that describes an energy landscape with a single minimum. The result for $\Delta = 0.1$ is shown in Fig. 4. The control parameters are the obstacle density $\alpha = M/N$ and size σ . If α is small, the tracer particle can easily find islands of configurations \mathbf{x} that satisfy all the constraints $h_\mu > 0$: the total potential energy U_N and the pressure vanish and the system is unjammed. The overlap $q < 1$ measures the typical distance between two zero-energy configurations. Upon increasing α , q increases and eventually

reaches $q = 1$ at α_J , which is the jamming transition point (Fig. 4). Naturally, due to the additional degrees of freedom when $\Delta > 0$, we have $\alpha_J(\Delta) > \alpha_J(0)$ for equal σ . For $\sigma > 0$, the RS ansatz is stable for all values of α and it describes the jamming transition. For $\sigma < 0$ instead, the jamming line is surrounded by a replica symmetry broken (RSB) region where the RS ansatz is unstable. The jamming transition should thus be described by the RSB ansatz where $q(x)$ is not constant, corresponding to a rough energy landscape. The qualitative behavior of the phase diagram is independent of Δ , in particular the jamming line for $\sigma < 0$ is always surrounded by a RSB region.

An important observable to characterize jamming is the gap distribution $\rho(h) \equiv \frac{1}{N} \sum_{\mu=1}^M \langle \delta(h_\mu - h) \rangle$ that also gives the contact number $z = \int_{-\infty}^0 dh \rho(h)$. At jamming, z counts the gaps h_μ that are exactly equal to zero. For comparison with numerical results, we introduce the positive gap distribution $g(h) \equiv \theta(h)\rho(h) / \int_0^\infty dh \rho(h)$, and the force distribution $P(f) \equiv \theta(-h)\rho(h) \frac{\partial h}{\partial f} / \int_{-\infty}^0 \rho(h) \frac{\partial h}{\partial f} df$, where $f = -h/p$ (corresponding to negative gaps), both normalized to 1. For the standard perceptron model with $\Delta = 0$ and $\sigma < 0$, jamming is isostatic with $z = 1$ (26), and both $g(h)$ and $P(f)$ exhibit a power law behavior (24–26). In the jammed phase and $\alpha \gtrsim \alpha_J$, the system is described by a “regular” full RSB solution where $1 - q(x) \sim y_x^2 x^{-2}$ for $q(x) \sim 1$, and $g(h)$ and $P(f)$ are regular and finite functions. The prefactor y_x is predominantly controlled by the contact number z , and diverges at isostaticity when $z = 1$ (26) and the regular solution breaks down. At α_J , the model is described by the “jamming” solution where $1 - q(x) \sim x^{-\kappa}$, $g(h) \sim h^{-\gamma}$ and $P(f) \sim f^\theta$, with critical exponents $\kappa \simeq 1.42$, $\gamma = (2 - \kappa)/\kappa$ and $\theta = (3\kappa - 4)/(2 - \kappa)$ (15, 24–26). Near α_J , the regular solution should connect to the jamming solution. This matching argument leads to $z - 1 \sim p^{1/2}$, which is the same scaling behavior of spherical particles (6).

The situation is completely different if $\Delta > 0$. One can show that the contact number at jamming is $z_J \geq 1$, meaning that the regular solution persists even at α_J . Consequently, $g(h)$ and $P(f)$ are finite and regular functions at jamming, and the square-root behavior of the contact number is replaced by $z - z_J = c_\Delta p$. At α_J , the regular solution should connect to the jamming solution in the limit of $\Delta \rightarrow 0$. Using the form of the scaling solution derived for $\Delta \rightarrow 0$ in (26) and $z - z_J \sim p$ this matching argument leads to the scaling behavior of $g(h)$ and $P(f)$ at α_J :

$$g(h) \sim \begin{cases} \Delta^{-\mu\gamma} p_0(h\Delta^{-\mu}) & (h \sim \Delta^\mu) \\ h^{-\gamma} & (h \sim 1) \end{cases}, \quad [14]$$

$$P(f) \sim \begin{cases} \Delta^{\theta\nu} p_0(f\Delta^{-\nu}) & (f \sim \Delta^\nu) \\ f^\theta & (f \sim 1) \end{cases}, \quad [15]$$

with new critical exponents $\mu = \kappa/(4\kappa - 4) = 0.851$, $\nu = \mu - 1/2$, and a universal scaling function $p_0(x)$. The scaling analysis also leads to $z_J - 1 \sim \Delta^{1/2}$ and $c_\Delta \sim \Delta^{-1/2}$, consistently with the marginal stability argument, Eqs. (8), (11).

The simplicity of the model allows us to derive the analytical form of the density of states $D(\omega)$. As before, we define the Hessian matrix as the second derivatives of the interaction potential V_N , Eq. (12) w.r.t x_i and R_μ/Δ . Using the Edwards-Jones formula for the eigenvalue density $\rho(\lambda)$ (51, 52), the

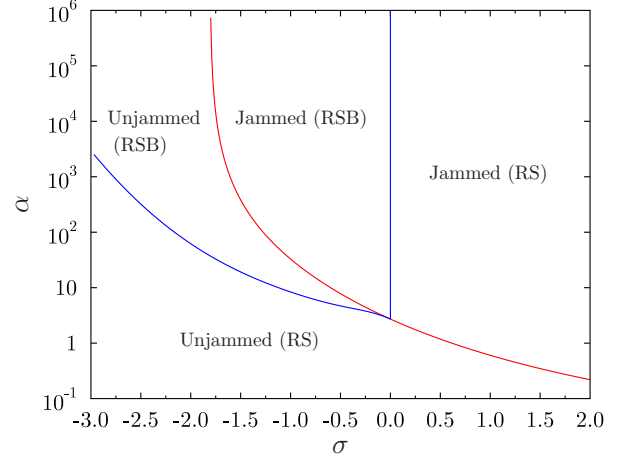


Fig. 4. The phase diagram of the perceptron model for $\Delta = 0.1$. The red line denotes the jamming point. The blue lines denote the RSB instability. The jamming line in the nonconvex region ($\sigma < 0$) is surrounded by the RSB lines.

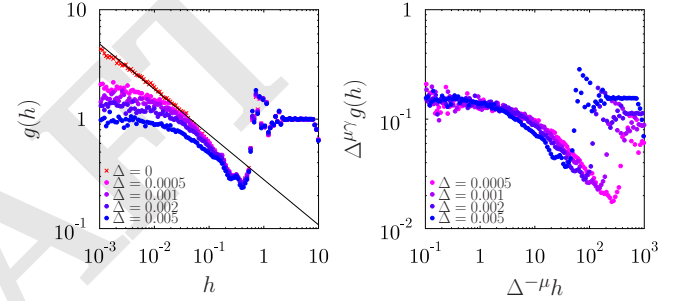


Fig. 5. Gap distribution $g(h)$ of breathing particles near the jamming point, $p = 10^{-6}$. (Left) Symbols denote the numerical result, while the full line denotes the theoretical prediction, $g(h) \propto h^{-0.413}$. (Right) Scaling plot of the same data according to Eq. (14).

density of states $D(\omega) = 2\omega\rho(\omega^2)$ can be expressed analytically in closed form as a function of z , k_R and p . These quantities should be obtained by solving numerically the full RSB equations but for simplicity, because here we are interested only in the scaling properties of $D(\omega)$, to obtain Fig. 2 we used arbitrary functions z , k_R and p which are compatible with the analytical scaling derived from the full RSB equation. We find that $D(\omega)$ displays three separate bands (Fig. 2). As in the standard perceptron (24), marginal stability in the full RSB phase implies that the lowest band starts from $\omega = 0$ and for small ω , $D(\omega) \sim \omega^2$. The lowest band terminates at $\omega_0 \sim \Delta^{1/2} p^{1/2}$ near which $D(\omega)$ exhibits a sharp peak. At $\omega_1 \sim \Delta$ a delta peak is found, while the highest band starts from $\omega_2 \sim \Delta^{1/2}$. The qualitative behavior of $D(\omega)$, and the scaling of ω_0 , ω_1 and ω_2 are the same of all the models displaying hypostatic jamming, such as ellipsoids (31, 32) and BP (43). This confirms that the generalised perceptron can reproduce analytically all the critical properties of the hypostatic jamming transition.

As a final check of universality, we test the prediction for the Δ dependence of the gap distribution function $g(h)$ at the jamming point, Eq. (14). In Fig. 5, we show numerical results (obtained as in (43)) for $g(h)$ of the BP model at $p = 10^{-5}$, a

value small enough to observe the critical behavior. Here, as usual for particle systems, $g(h)$ is normalized by $g(h) \rightarrow 1$ for larger h . When $\Delta = 0$, $g(h)$ exhibits a power law divergence, $g(h) \sim h^{-\gamma}$, where $\gamma = 0.413$, consistently with previous numerical observation (6, 14, 15). For finite Δ , on the contrary, the divergence of $g(h)$ is cutoff (Fig. 5), consistently with the theoretical prediction of Eq. (14).

Conclusions – Using a marginal stability argument, we derived the scaling behavior of the contact number z and the density of states $D(\omega)$ of ellipsoids and breathing particles. Our theory predicts that the scaling behaviors of the two models are identical, which we confirmed numerically. Many other models of non-spherical particles display the same jamming criticality (40), which defines a new universality class of hypostatic jamming. We introduced an analytically solvable model which allows us to derive analytically the critical exponents associated to the new universality class.

One of the most surprising output of our theory is the universality of the density of states $D(\omega)$ (Fig. 2). This might be relevant for some colloidal experiments where the constituents are non-spherical (53), in which the vibrational modes could be experimentally extracted from the fluctuations of positions (54, 55). Another relevant question is how non-spherical particles would flow under shear (30). The divergence of the viscosity at jamming is related to the low eigenvalues of $D(\omega)$ (56), which suggests that the shear flow of non-spherical particles should be quite different from that of spherical particles, in agreement with recent experiments (57).

ACKNOWLEDGMENTS. We thank B. Chakraborty, A. Ikeda, J. Kurchan, S. Nagel and S. Franz for interesting discussions. This project has received funding from the European Research Council (ERC) under the European Union’s Horizon 2020 research and innovation programme (grant agreement n.723955-GlassUniversality). This work was supported by a grant from the Simons Foundation (#454953, Matthieu Wyart and #454955, Francesco Zamponi) and by “Investissements d’Avenir” LabEx PALM (ANR-10-LABX-0039-PALM, P. Urbani). We thank the authors of Refs. (40) and (32) for sharing their data used in Figs. 1 and 2.

1. Liu AJ, Nagel SR, van Saarloos W, Wyart M (2010) *The jamming scenario: an introduction and outlook*, eds. L.Berthier, Biroli G, Bouchaud J, Cipelletti L, van Saarloos W. (Oxford University Press, Oxford).
2. Van Hecke M (2009) Jamming of soft particles: geometry, mechanics, scaling and isotaticity. *Journal of Physics: Condensed Matter* 22(3):033101.
3. Torquato S, Stillinger FH (2010) Jammed hard-particle packings: From kepler to bernal and beyond. *Rev. Mod. Phys.* 82(3):2633–2672.
4. Bernal J, Mason J (1960) Packing of spheres: co-ordination of randomly packed spheres. *Nature* 188(4754):910.
5. Durian DJ (1995) Foam mechanics at the bubble scale. *Phys. Rev. Lett.* 75(26):4780–4783.
6. O’Hern CS, Silbert LE, Liu AJ, Nagel SR (2003) Jamming at zero temperature and zero applied stress: The epitome of disorder. *Phys. Rev. E* 68(1):011306.
7. Zhang Z, et al. (2009) Thermal vestige of the zero-temperature jamming transition. *Nature* 459(7244):230.
8. Karayiannis NC, Foteinopoulou K, Laso M (2009) The structure of random packings of freely jointed chains of tangent hard spheres. *The Journal of chemical physics* 130(16):164908.
9. Donev A, et al. (2004) Improving the density of jammed disordered packings using ellipsoids. *Science* 303(5660):990–993.
10. Jaoshvili A, Esakia A, Porrati M, Chaikin PM (2010) Experiments on the random packing of tetrahedral dice. *Phys. Rev. Lett.* 104(18):185501.
11. Bi D, Lopez J, Schwarz J, Manning ML (2015) A density-independent rigidity transition in biological tissues. *Nature Physics* 11(12):1074.
12. O’Hern CS, Langer SA, Liu AJ, Nagel SR (2002) Random packings of frictionless particles. *Physical Review Letters* 88(7):075507.
13. Ellenbroek WG, Somfai E, van Hecke M, van Saarloos W (2006) Critical scaling in linear response of frictionless granular packings near jamming. *Phys. Rev. Lett.* 97(25):258001.
14. Donev A, Torquato S, Stillinger FH (2005) Pair correlation function characteristics of nearly jammed disordered and ordered hard-sphere packings. *Phys. Rev. E* 71(1):011105.
15. Charbonneau P, Kurchan J, Parisi G, Urbani P, Zamponi F (2014) Fractal free energy landscapes in structural glasses. *Nat. Commun.* 5:3725.
16. Charbonneau P, Corwin EI, Parisi G, Zamponi F (2015) Jamming criticality revealed by removing localized buckling excitations. *Phys. Rev. Lett.* 114(12):125504.

17. Wyart M, Silbert LE, Nagel SR, Witten TA (2005) Effects of compression on the vibrational modes of marginally jammed solids. *Phys. Rev. E* 72(5):051306.
18. Wyart M (2005) On the rigidity of amorphous solids. *arXiv preprint cond-mat/0512155*.
19. Maxwell JC (1864) L. on the calculation of the equilibrium and stiffness of frames. *The London, Edinburgh, and Dublin Philosophical Magazine and Journal of Science* 27(182):294–299.
20. Brito C, Wyart M (2006) On the rigidity of a hard-sphere glass near random close packing. *EPL* 76(1):149.
21. Wyart M (2012) Marginal stability constrains force and pair distributions at random close packing. *Phys. Rev. Lett.* 109(12):125502.
22. Lerner E, Düring G, Wyart M (2013) Low-energy non-linear excitations in sphere packings. *Soft Matter* 9(34):8252–8263.
23. DeGiuli E, Lerner E, Brito C, Wyart M (2014) Force distribution affects vibrational properties in hard-sphere glasses. *Proceedings of the National Academy of Sciences* 111(48):17054–17059.
24. Franz S, Parisi G, Urbani P, Zamponi F (2015) Universal spectrum of normal modes in low-temperature glasses. *PNAS* 112(47):14539–14544.
25. Franz S, Parisi G (2016) The simplest model of jamming. *Journal of Physics A: Mathematical and Theoretical* 49(14):145001.
26. Franz S, Parisi G, Sevelev M, Urbani P, Zamponi F (2017) Universality of the SAT-UNSAT (jamming) threshold in non-convex continuous constraint satisfaction problems. *SciPost Phys.* 2(3):019.
27. Man W, et al. (2005) Experiments on random packings of ellipsoids. *Phys. Rev. Lett.* 94(19):198001.
28. Delaney G, Weaire D, Hutzler* S, Murphy S (2005) Random packing of elliptical disks. *Philosophical Magazine Letters* 85(2):89–96.
29. Donev A, Connelly R, Stillinger FH, Torquato S (2007) Underconstrained jammed packings of nonspherical hard particles: Ellipses and ellipsoids. *Phys. Rev. E* 75(5):051304.
30. Mailman M, Schreck CF, O’Hern CS, Chakraborty B (2009) Jamming in systems composed of frictionless ellipse-shaped particles. *Phys. Rev. Lett.* 102(25):255501.
31. Zeravcic Z, Xu N, Liu A, Nagel S, van Saarloos W (2009) Excitations of ellipsoid packings near jamming. *EPL (Europhysics Letters)* 87(2):26001.
32. Schreck CF, Mailman M, Chakraborty B, O’Hern CS (2012) Constraints and vibrations in static packings of ellipsoidal particles. *Phys. Rev. E* 85(6):061305.
33. Williams SR, Philippe AP (2003) Random packings of spheres and spherocylinders simulated by mechanical contraction. *Phys. Rev. E* 67(5):051301.
34. Blououloff J, Fraden S (2006) The coordination number of granular cylinders. *EPL (Europhysics Letters)* 76(6):1095.
35. Wouterse A, Williams SR, Philippe AP (2007) Effect of particle shape on the density and microstructure of random packings. *Journal of Physics: Condensed Matter* 19(40):406215.
36. Wouterse A, Luding S, Philippe A (2009) On contact numbers in random rod packings. *Granular Matter* 11(3):169–177.
37. Marschall T, Teitel S (2018) Compression-driven jamming of athermal frictionless spherocylinders in two dimensions. *Phys. Rev. E* 97(1):012905.
38. Jiao Y, Stillinger FH, Torquato S (2010) Distinctive features arising in maximally random jammed packings of superballs. *Phys. Rev. E* 81(4):041304.
39. Delaney GW, Cleary PW (2010) The packing properties of superellipsoids. *EPL* 89(3):34002.
40. VanderWerf K, Jin W, Shattuck MD, O’Hern CS (2018) Hypostatic jammed packings of frictionless nonspherical particles. *Phys. Rev. E* 97(1):012909.
41. Boromand A, Signoriello A, Ye F, O’Hern CS, Shattuck M (2018) Jamming of deformable polygons. *arXiv preprint arXiv:1801.06150*.
42. Baulé A, Mari R, Bo L, Portal L, Makse HA (2013) Mean-field theory of random close packings of axisymmetric particles. *Nat. Commun.* 4:2194.
43. Brito C, Lerner E, Wyart M (2018) Theory for swap acceleration near the glass and jamming transitions. *arXiv preprint arXiv:1801.03796*.
44. Ninarello A, Berthier L, Coslovich D (2017) Models and algorithms for the next generation of glass transition studies. *Phys. Rev. X* 7(2):021039.
45. Alexander S (1998) Amorphous solids: their structure, lattice dynamics and elasticity. *Physics reports* 296(2-4):65–236.
46. Gay J, Berne B (1981) Modification of the overlap potential to mimic a linear site–site potential. *The Journal of Chemical Physics* 74(6):3316–3319.
47. Yan L, DeGiuli E, Wyart M (2016) On variational arguments for vibrational modes near jamming. *EPL (Europhysics Letters)* 114(2):26003.
48. Schreck CF, Xu N, O’Hern CS (2010) A comparison of jamming behavior in systems composed of dimer- and ellipse-shaped particles. *Soft Matter* 6(13):2960–2969.
49. Goodrich CP, Liu AJ, Nagel SR (2012) Finite-size scaling at the jamming transition. *Physical review letters* 109(9):095704.
50. Mézard M, Parisi G, Virasoro M (1987) *Spin glass theory and beyond: An Introduction to the Replica Method and Its Applications*. (World Scientific Publishing Company) Vol. 9.
51. Edwards SF, Jones RC (1976) The eigenvalue spectrum of a large symmetric random matrix. *Journal of Physics A: Mathematical and General* 9(10):1595.
52. Livan G, Novaes M, Vivo P (2017) Introduction to random matrices theory and practice. *arXiv preprint arXiv:1712.07903*.
53. Kim JW, Larsen RJ, Weitz DA (2006) Synthesis of nonspherical colloidal particles with anisotropic properties. *Journal of the American Chemical Society* 128(44):14374–14377.
54. Chen K, et al. (2010) Low-frequency vibrations of soft colloidal glasses. *Phys. Rev. Lett.* 105(2):025501.
55. Ghosh A, Chikkadi VK, Schall P, Kurchan J, Bonn D (2010) Density of states of colloidal glasses. *Phys. Rev. Lett.* 104(24):248305.
56. Lerner E, Düring G, Wyart M (2012) A unified framework for non-brownian suspension flows and soft amorphous solids. *Proceedings of the National Academy of Sciences*.
57. Tapia F, Shaikh S, Butler JE, Pouliquen O, Guazzelli E (2017) Rheology of concentrated suspensions of non-colloidal rigid fibres. *Journal of Fluid Mechanics* 827.